

Effect of Temperature and Strain Rate on the Compressive Flow of Aluminum Composites Containing Submicron Alumina Particles

M. KOUZELI and D.C. DUNAND

Uniaxial compression tests were conducted on aluminum composites containing 34 and 37 vol pct submicron alumina particles, to study the effect of temperature and strain rate on their flow stress. For temperatures between 25 °C and 600 °C and strain rates between 10^{-3} and 1 s^{-1} , the flow stress of the composites is significantly higher than that of unreinforced aluminum tested under similar conditions. This can be attributed to direct strengthening of the composites due to load sharing between the particles and the matrix, and an enhanced *in-situ* matrix flow stress resulting from a particle-induced increase in dislocation density. The composites, however, exhibit the same stress dependence on temperature and strain rate as unreinforced aluminum, indicating a common hardening mechanism, *i.e.*, forest dislocation interactions. The forest hardening present under the explored testing conditions masks the effects of direct dispersion strengthening operative at lower deformation rates in these materials.

I. INTRODUCTION

A dispersion of submicron oxide particles in a metal enhances both its low-temperature and high-temperature mechanical properties.^[1] The volume fraction of submicron dispersoids in metals is usually less than 10 vol pct, limited by the powder-metallurgy processing techniques used in their production. Consequently, continuum strengthening in the form of load sharing between the matrix and the dispersoids is small enough to be neglected, and the effect of the particles on the mechanical properties of dispersion-strengthened metals can be understood by consideration of dislocation-particle interactions.^[2]

In recent years, novel processing techniques have led to the production of aluminum containing concentrated dispersions of submicron alumina particles. In particular, liquid metal infiltration can produce dispersion-strengthened cast aluminum (DSC-Al*) containing 20 to 60 vol pct submi-

*DSC-Al is a trademark of Chesapeake Composites Corp., New Castle, DE.

cron oxide particles.^[3,4] The combination of large volume fractions and small size of the particles in these metal-ceramic composites results in both continuum composite strengthening and strong dislocation-particle interactions, making these materials interesting hybrids between metal-matrix composites and dispersion-strengthened metals.

The creep behavior of DSC-Al with 25 vol pct alumina particles has been studied both experimentally and theoretically.^[5,6] For strain rates between 10^{-9} and 10^{-3} s^{-1} , the superior creep resistance of DSC-Al, as compared to precipitation-strengthened aluminum alloys, can be attributed to the existence of a threshold stress below which creep by

dislocation climb is negligible. This threshold stress was shown to be a result of the interaction between dislocations and alumina particles acting as dispersoids, and was theoretically calculated after consideration of the stress exerted on a dislocation in the process of detachment from a dispersoid by dislocation pileups at the same and other dispersoids. In these studies, the possible enhancement of creep resistance due to load partitioning between the aluminum matrix and the alumina particles was not considered, because the elasto-plastic mismatch necessary for load transfer was assumed relaxed by local diffusional processes around the dispersoids. Increased creep resistance due to load partitioning, however, has been reported in metal-matrix composites with similar volume fractions of larger ceramic particles tested at similar strain rates,^[7,8,9] for which relaxation is slower because of larger diffusion distances. Furthermore, in a recent study on DSC-Al tested in compression at 10^{-3} s^{-1} ,^[10] it was shown that significant enhancements in the elasto-plastic properties of these materials with respect to aluminum are a product of composite strengthening (*i.e.*, load transfer).

The purpose of the present study is to identify the micro-mechanisms of flow in DSC-Al at strain rates greater than those previously reported in the creep regime,^[5,6] in this elevated strain-rate regime, load transfer between the metal and ceramic phase must be taken into account. To this end, compression tests are conducted at temperatures between 25 °C and 600 °C and at relatively elevated strain rates between 10^{-3} and 1 s^{-1} (typical of forming operations), on DSC-Al specimens containing 34 and 37 vol pct submicrometer alumina particles. A continuum-mechanics load-transfer model, which is presented in a separate publication,^[10] is then used to assess the *in-situ* flow stress of the aluminum matrix in these materials at each testing condition. These *in-situ* flow stresses are rationalized in the context of theories for the thermodynamics and kinetics of slip and compared to the flow stresses of bulk aluminum at similar temperatures and strain rates, as reported in the literature. We show that, in the temperature and strain-rate regime investigated,

M. KOUZELI, Postdoctoral Fellow, and D.C. DUNAND, Professor, are with the Department of Materials Science and Engineering, Northwestern University, Evanston, IL 60208. Contact e-mail: dunand@northwestern.edu
Manuscript submitted March 10, 2003.

the observed temperature and rate dependence of flow in the matrix of the present composites is controlled by the same mechanism as in unreinforced aluminum, *i.e.*, forest dislocation interactions.

II. EXPERIMENTAL PROCEDURES

Two cast billets of DSC-Al consisting of 99.9 pct pure aluminum with 34 and 37 vol pct α -Al₂O₃ particles were supplied by Chesapeake Composites Corp. (New Castle, DE); the two materials will be referred to as IPC34 and IPC37, consistent with Reference 10 (IPC stands for interpenetrating phase composite). The alumina particles have a mean diameter of 0.3 μ m, and were partially sintered to form a self-supporting preform before they were infiltrated with liquid aluminum.¹³¹

Uniaxial compressive testing was conducted on cylindrical samples 10 mm in diameter and 15 mm in height. The samples were deformed between polished WC/Co platens in a 100 kN servohydraulic universal testing machine outfitted with a controlled atmosphere chamber and a furnace. The testing machine was operated under constant crosshead displacement, at initial strain rates of 10⁻³, 10⁻², 10⁻¹, and 1 s⁻¹. Measured strain rates throughout a single test never varied by more than a factor of 1.3. Strain in the samples was determined from the crosshead displacement, corrected for the (temperature-dependent) compliance of the testing setup. Polytetrafluoroethylene was used as a lubricant between the sample and the platen surfaces for temperatures up to 250 °C, and BN was used at higher temperatures.

For experiments above ambient temperature, the testing chamber was first evacuated and flushed with argon to avoid oxidation of the WC/Co platens, then heated at 10 °C/min to the specific testing temperature (250 °C, 500 °C or 600 °C) and left to equilibrate for 45 minutes prior to testing. The temperature dependence of the flow stress for both IPC34 and IPC37 was determined for a nominal strain rate of 10⁻³ s⁻¹, while the strain-rate dependence of the flow stress was determined for IPC34 at 25 °C, 250 °C, and 500 °C, and for IPC37 at 25 °C.

III. RESULTS

The microstructure of IPC34 and IPC37 is characterized by a near-homogeneous distribution of fine alumina particles in a pore-free aluminum matrix (Figure 1). Inhomogeneities exist on a scale much coarser than the particle size in the form of particle-rich spheres, approximately 100 μ m in diameter, separated by narrow channels of particle-poor matrix (Figure 1). These spheres are probably produced during spray drying of the particle slurry prior to sintering.¹³¹ As a result of sintering, the ceramic particles in the present DSC-Al are not discrete dispersoids but form an interconnected network throughout the microstructure. Since both metal and ceramic phases are contiguous in three dimensions, these DSC-Al materials are interpenetrating phase composites.¹¹⁰¹

Typical compressive flow curves of IPC34 and IPC37 at different temperatures and strain rates are given in Figure 2. As in pure aluminum, increasing the strain rate and decreasing the temperature serves to increase the flow stress of these materials. Increasing the volume fraction of particles also

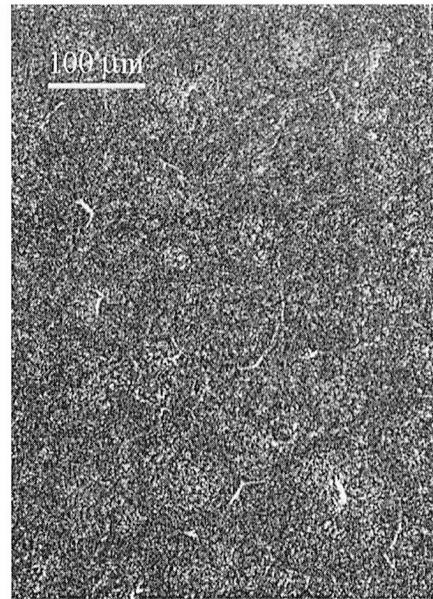


Fig. 1—Optical micrograph of material IPC37. The lighter phase is aluminum and the darker phase is alumina.

leads to an increase in the flow stress (Figure 2(a)). A typical characteristic of all measured stress-strain curves is the existence of an instability, characterized by a peak stress after which the values of stress continuously decrease. This strain-softening phenomenon, which is related to the damage of the interconnected network of alumina particles during straining, is discussed in detail elsewhere.¹¹⁰¹ In the present study, we compare the stress at 1 pct strain ($\sigma_{1\%}$) to investigate the temperature and strain-rate dependence of the flow stress without ambiguity; at this strain, damage is small enough to be ignored and flow has not yet become unstable.

The value of $\sigma_{1\%}$ is plotted as a function of temperature in Figure 3(a), and as a function of strain rate in Figure 3(b). The strain-rate-sensitivity parameter, m , commonly defined¹¹¹ as the slope of the curves in Figure 3(b), increases with temperature from 0.010 at 25 °C to 0.10 at 500 °C for IPC34. An increase in the volume fraction of particles also results in a slight increase of m at 25 °C ($m = 0.010$ for IPC34 and $m = 0.012$ for IPC37). The values of m at 25 °C for the present materials compare well with values reported in the literature for pure aluminum in the same strain-rate regime, which are approximately 0.01.¹¹²¹ The stresses in the present materials, however, are an order of magnitude higher than in pure aluminum.

IV. DISCUSSION

A. Composite vs Matrix Flow Stress

Composite strengthening, in the form of load transfer from the aluminum matrix to the alumina particles, cannot be ignored in the present study, due to the large volume fractions of particles, the interconnected nature of these particles, and the relatively high strain rates at which deformation takes place. An illustration of the relative contribution of load partitioning in the present materials is the magnitude of their Young's modulus: 127 and 135 GPa at room temperature for

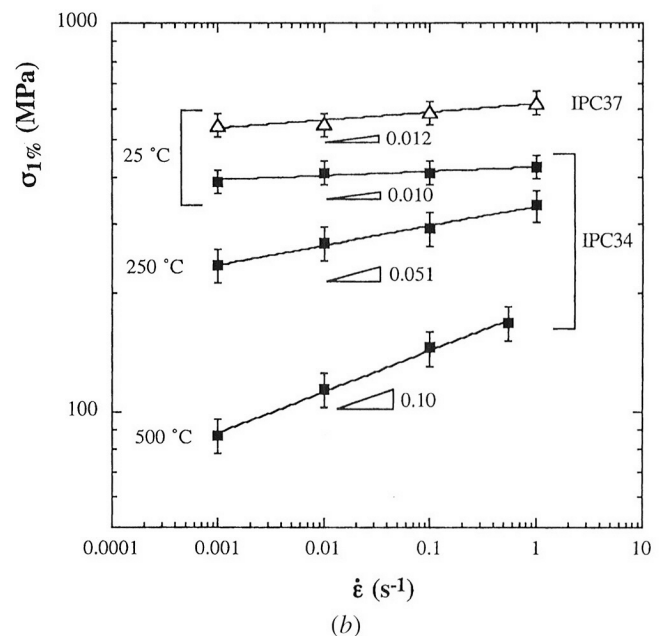
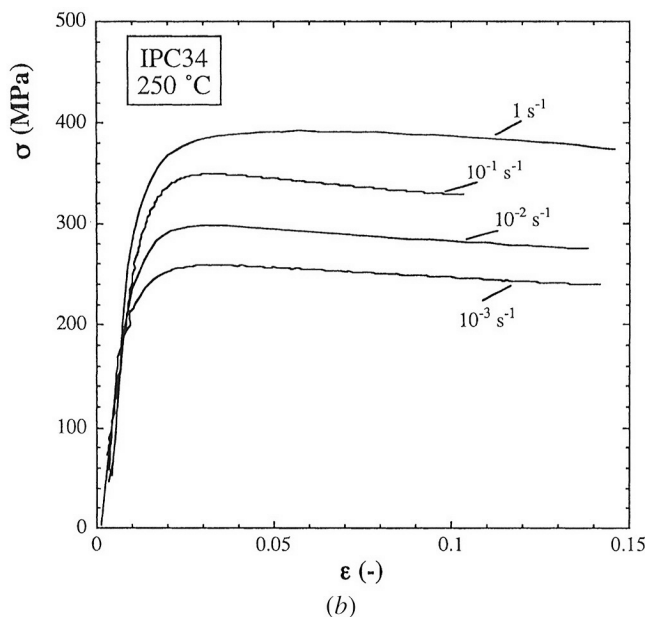
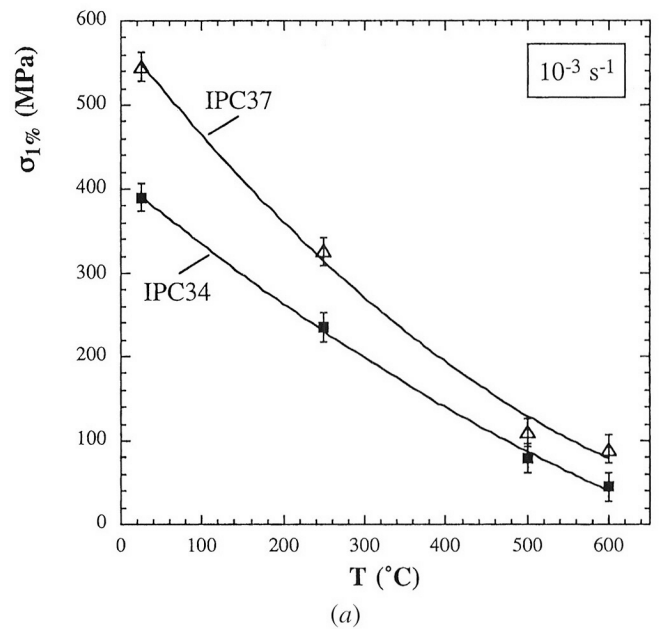
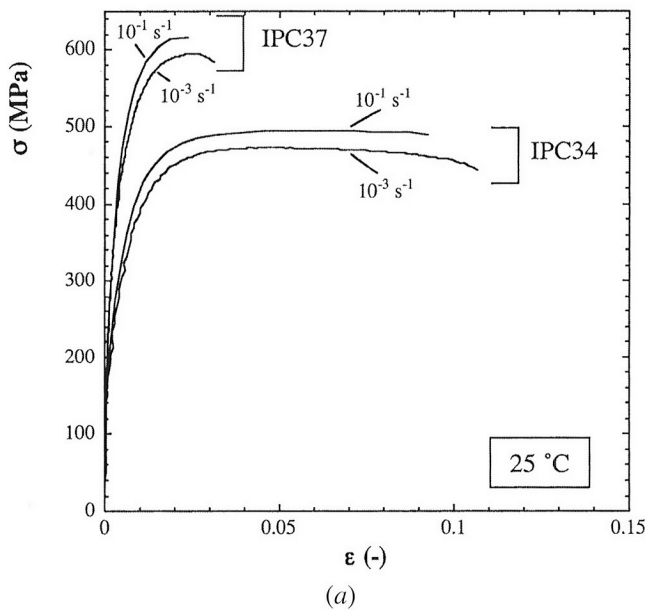


Fig. 2—True stress-strain curves at various strain rates for (a) ambient temperature and (b) 250 °C. Absolute compressive values of stress and strain are plotted.

Fig. 3—The stress at 1 pct strain ($\sigma_{1\%}$) as a function of (a) temperature at 10^{-3} s^{-1} and (b) strain rate at various temperatures. The values plotted are averages of three tests.

IPC34 and IPC37, respectively, almost double that of pure aluminum (69 GPa).¹¹⁰¹ The specifics of elasto-plastic load partitioning between matrix and particles (discussed in more detail in Reference 10) depend on, among other things, the volume fraction of particles and the testing temperature; an increase in the values of these parameters results in the stiff alumina particles carrying a relatively larger proportion of the load. Thus, to understand the influence of temperature and strain rate on plastic flow in the present composites, any ambiguity related to different load-sharing conditions at different testing conditions and different volume fractions must be eliminated by considering the *in situ* matrix stress, computed and analyzed as described in the following.

In a previous publication,¹¹⁰¹ it was shown that the classical self-consistent (CSC) model, based on a continuum approach

to load transfer, successfully describes the effects of reinforcement volume fraction and interconnectivity on the elastic and plastic properties of IPC34 and IPC37, both at ambient and elevated temperatures. In the present study, we use this model to calculate the flow stress of the aluminum matrix from the composite flow stress, as illustrated in Figure 4 for IPC34 at 25 °C. From the resulting matrix flow curves, the matrix stress at a matrix strain $\epsilon^m = 0.015$ is determined, which corresponds to a composite strain $\epsilon^c = 0.010$, as computed from the CSC model. In the framework of the self-consistent approaches, the effective medium in which the individual constituents of the composite are embedded is the composite itself. Thus, the influence of constrained

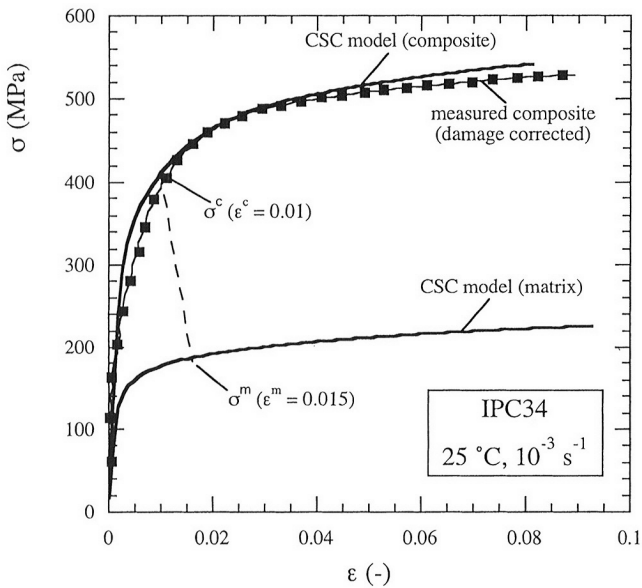


Fig. 4—Stress-strain curve for IPC34 at 25 °C and 10^{-3} s^{-1} (experiment and CSC model) and matrix stress-strain curve calculated from CSC model.^[10]

plastic flow due to enhanced levels of stress triaxiality is taken into account, and the matrix flow stress is not over-estimated, as can be the case when the matrix itself is taken as the effective medium.

B. Rate-Dependent Plasticity

The interaction of mobile, gliding dislocations with obstacles, such as other dislocations or particles, determines the flow stress of a metal at a given strain rate. Dislocation glide is a kinetic process determined by the rate at which dislocations are thermally activated through, or around, obstacles. Dislocation climb is not considered in the present discussion due to the high strain rates involved; deformation under creeping conditions is climb controlled in the present materials and a different modeling approach must be taken.^[5,6] The development of rate equations for obstacle-controlled plasticity by dislocation glide has been studied for many years, and a different set of equations corresponds to each type of obstacle,^[13] making the identification of the controlling mechanisms difficult. It was pointed out by Frost and Ashby,^[14] however, that obstacles fall into three broad classes, depending on the strength of their interaction with moving dislocations: (1) strong obstacles (including dispersoids and large or strong precipitates), (2) medium strength obstacles (including forest dislocations, radiation damage, and small or weak precipitates), and (3) weak obstacles (including lattice resistance and solid-solution hardening). To determine the type of obstacle controlling dislocation glide in the matrix of DSC-Al, we analyze our data based on this traditional phenomenological approach for describing thermal activation over a barrier.

The strength of a specific class of obstacles is generally characterized by the activation energy ΔF required for a moving dislocation to overcome an obstacle without an externally applied stress, and the athermal flow stress $\hat{\tau}$,

which is the stress needed to overcome the obstacle without the aid of thermal energy. These parameters are functions of the shear modulus, μ , and the magnitude of the Burger's vector, b :

$$\Delta F = \beta \mu b^3 \quad [1]$$

and

$$\hat{\tau} = \alpha \frac{\mu b}{l} \quad [2]$$

where l is the obstacle spacing. The constants α and β are indicative of the obstacle strength and distribution; for example, values of $\alpha > 1$ and $\beta \approx 2$ are characteristic of strong obstacles such as dispersoids, whereas $\alpha \approx 1$ and $\beta \approx 0.2$ correspond to medium strength obstacles such as forest dislocations.^[13,14]

Assuming a regular array of obstacles, consideration of both the temperature and strain rate contributions to the kinetics of slip leads to the following relationship between shear strain rate $\dot{\gamma}$, temperature T , and the shear stress σ_s :

$$\dot{\gamma} = \dot{\gamma}_0 \exp \left[-\frac{\Delta F}{kT} \left(1 - \frac{\sigma_s}{\hat{\tau}} \right) \right] \quad [3]$$

where k is the Boltzman constant. The pre-exponential term $\dot{\gamma}_0$ is determined by the frequency of attempts to overcome an obstacle, and is usually considered a constant with values ranging between 10^5 and 10^{10} s^{-1} .^[14,15] Combining Eqs. [1] through [3], and rearranging, yields

$$\frac{\sigma_s}{\mu} = \frac{\alpha b}{l} - \frac{\alpha b \ln(\dot{\gamma}_0/\dot{\gamma})}{\beta l (\mu b^3/kT)} \quad [4]$$

In Figure 5(a), the matrix stress at $\varepsilon^m = 0.015$, calculated from the CSC model as illustrated in Figure 4, is plotted against the testing parameters according to Eq. [4], after transformation of the uniaxial stress σ and strain rate $\dot{\varepsilon}$ to a shear stress and shear strain rate ($\sigma_s^m = \sigma^m/\sqrt{3}$, and $\dot{\gamma} = \sqrt{3}\dot{\varepsilon}$). The temperature dependence of μ is taken into consideration following the relationship^[14]

$$\mu = \mu_0 \left(1 + \frac{(T - 300) T_M}{T_M} \frac{d\mu}{\mu_0 dT} \right) \quad [5]$$

where μ_0 is the shear modulus at 300 K, T_M is the melting point, and T is the temperature in Kelvin. The temperature dependence of b is calculated from the data for the variation with temperature of the lattice parameter a for Al, given in Ref. [16], and the relationship between b and a for an fcc structure ($b = a/\sqrt{2}$). The parameter $\dot{\gamma}_0$ is set to 10^6 s^{-1} in accordance with Reference 14; it is worth noting that varying $\dot{\gamma}_0$ within its permissible range does not change the linearity of the data in Figure 5(a) for IPC34 and IPC37, unlike the results reported in Reference 15 for pure aluminum.

A linear correlation for the two data sets is observed in Figure 5(a), indicating that Eq. [3] provides a good description of the effects of strain rate and temperature on the matrix flow stress of IPC34 and IPC37. The simplifying assumption of a regular array of obstacles used to derive Eq. [3]—instead of a random array, which is closer to reality—does not strongly affect the observed corre-

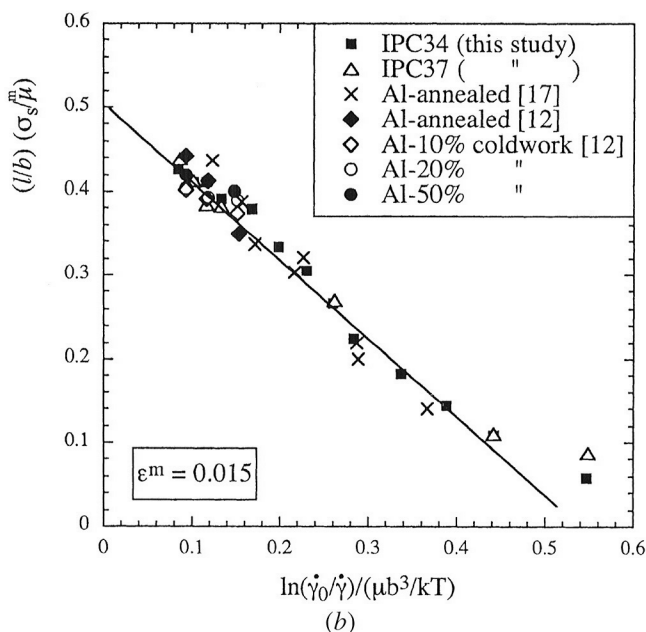
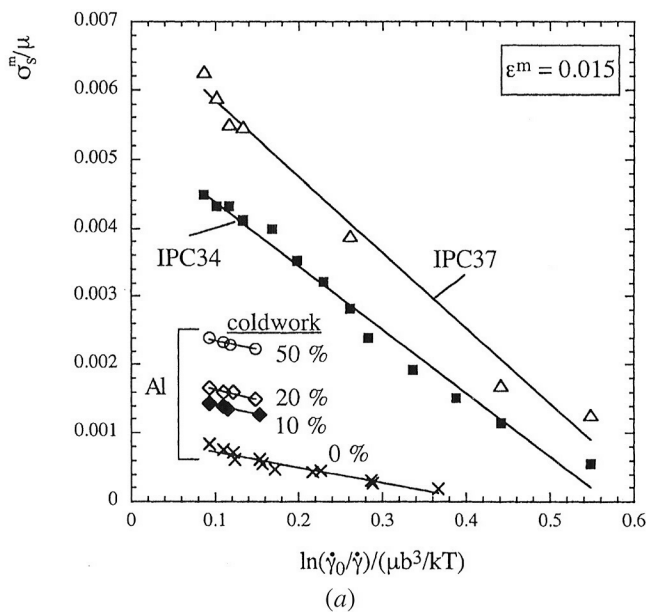


Fig. 5—(a) Experimental data for IPC34 and IPC37 and data from the literature for aluminum plotted according to Eq. [4], showing linear trends. (b) Same data plotted with the y-axis normalized by the obstacle spacing, l . The stress is the matrix (or pure aluminum) stress at $\epsilon^m = 0.015$.

lation. The data were also plotted according to the general form of Eq. [3]:^[14]

$$\dot{\gamma} = \dot{\gamma}_0 \exp \left[-\frac{\Delta F}{kT} \left(1 - \frac{\sigma_s}{\hat{\tau}} \right)^p \right]^q \quad [6]$$

which allows for a random distribution of obstacles and also for a variety of obstacle shapes; the parameters p and q of Eq. [6] were used as fitting parameters (within their permissible bounds^[14]). This exercise offered no improvement to the correlation factor of the experimental data. Kocks,^[15] however, demonstrated an improvement in linearity when the square root of both axes in Figure 5(a)

is taken, equivalent to taking $p = q = 1/2$ in Eq. [6]. A possible explanation is that Kocks compared the stress at the point where $d\sigma/d\epsilon = 0$, while we use the stress at a given strain ($\epsilon^m = 0.015$).

The value of the proportionality constant β in Eq. [1] can be determined by dividing the y intercept ($\alpha b/l$) with the magnitude of the slope ($\alpha b/\beta l$) of the lines in Figure 5(a), which are best linear fits through the data points corresponding to IPC34 and IPC37. For the aluminum matrix of these two materials, the value of β is nearly the same and equals 0.6. According to Ashby's scheme, this would indicate an activation energy characteristic of forest dislocation interactions, Eq. [1]. We compare this result with data from the literature on the temperature and strain-rate sensitivity of pure aluminum in the annealed state and after various amounts of cold work.^[12,17] For the purpose of direct comparison, the stress at 0.015 strain is extracted from these references at similar temperatures and strain rates as the present study (Figure 5(a)). The values of β calculated for the pure aluminum data below 50 pct cold work are also close to 0.5 (± 0.2), as expected for a fcc metal.

Calculation of the proportionality constant α in Eq. [2], on the other hand, requires knowledge of the obstacle spacing l and, thus, cannot be uniquely determined. For dispersion-strengthened aluminum, the interparticle distance is the most obvious candidate for obstacle separation. The calculated values for the activation energy $\Delta F \approx 0.6 \mu b^3$, however, indicate that the governing micromechanisms of flow in these materials are dislocation-dislocation interactions and not dislocation-dispersoid interactions (for which $\Delta F \approx 2\mu b/l$). Under the assumption that dislocation-dislocation interactions indeed govern flow, the average forest dislocation spacing should be used as the obstacle spacing in the calculation of α for the DSC-Al data and the pure aluminum data alike, making the value of this spacing the only differentiating parameter between the matrix of DSC-Al and pure aluminum. To check this hypothesis, we normalize the y-axis of Figure 5(a) by appropriate values of l/b for pure aluminum data, and choose values of l/b that make the DSC-Al data collapse onto the same curve. Such a normalization is presented in Figure 5(b), where, for aluminum cold worked to 0, 10, 20, and 50 pct, l is set at 170, 80, 70, and 50 nm, respectively, according to values cited in the literature.^[14,18] Using l values of 30 and 20 nm for IPC34 and IPC37, respectively, makes the DSC-Al lines fall on the same curve as the data for pure aluminum (Figure 5(b)), verifying the similarity in the flow-controlling mechanisms for the matrix of DSC-Al and pure aluminum. The only exceptions are the DSC-Al data points at 600 °C that do not seem to fit this line; we attribute this discrepancy to the dominance of thermally activated cross-slip at this temperature, a mechanism which for simplicity has been ignored in the present analysis. The intercept with the y-axis of the line in Figure 5(b) is the proportionality constant α (Eq. [2]), which equals 0.5, consistent with the original hypothesis that forest dislocation interactions are dominant in the matrix of the DSC-Al, rather than dislocation-dispersoid interactions with $\alpha > 1$.^[14] In what follows, we explore the reasons for similarity in flow-controlling mechanisms between the matrix of the DSC-Al materials and pure aluminum, and comment on the values for the forest dislocation spacing for the former, extrapolated from the preceding analysis.

In the present DSC-AI for the present testing conditions, dispersoids do not seem to directly control matrix dislocation motion. Usually, a dispersion of strong particles forces dislocations to bow between the particles, resulting in an activation energy that is so large that the resulting flow stress is almost athermal. If, however, a dispersion-strengthened metal is sufficiently work hardened, the flow stress of its matrix regains the temperature dependence that characterizes forest hardening.¹¹⁴ This initially work-hardened state may be the reason why matrix deformation in the present materials is dictated by forest dislocation interactions. The mismatch in the coefficients of thermal expansion of matrix and particles results in the punching of dislocations into the metal matrix during cooldown from the processing temperature.¹²¹ Furthermore, the plastic mismatch between matrix and particles results in the rapid accumulation of geometrically necessary dislocations with strain.¹⁹¹ Both the thermal dislocation density, ρ_{TH} , and the density of geometrically necessary dislocations, ρ_G , are quite high for the present materials owing to the large volume fraction of submicron particles they contain. The dislocation density ρ_{TH} was estimated to be 2×10^{14} and $3 \times 10^{14} \text{ m}^{-2}$ at 25 °C for IPC34 and IPC37, respectively, using the formula²⁰¹

$$\rho_{TH} = \frac{12 V_p \Delta CTE \Delta T}{(1 - V_p) b D} \quad [7]$$

where V_p is the volume fraction of particles, ΔCTE is the difference in coefficient of thermal expansion between matrix and particles, and D is the particle diameter. Similarly, the values for ρ_G for these two materials were estimated to be 11×10^{14} and $12 \times 10^{14} \text{ m}^{-2}$ at a strain $\epsilon^m = 0.015$ using the formula¹⁹¹

$$\rho_G = \left(\frac{V_p}{D} \right) \frac{4\sqrt{3} \epsilon^m}{b} \quad [8]$$

The average spacing l for these dislocations can be determined from the total dislocation density (sum of ρ_{TH} and ρ_G), as¹¹⁴

$$l = \frac{1}{\sqrt{\rho_{TH} + \rho_G}} \quad [9]$$

giving values of $l = 28$ and 26 nm for IPC34 and IPC37, respectively. As compared to the best-fit values ($l = 30$ and 20 nm) determined from the preceding experimental data, these values are in surprisingly good agreement, given the simplifying assumptions used to derive Eqs. [7] through [9]. We thus conclude that, from a microstructural viewpoint, the deformation behavior of the matrix of DSC-AI materials is only indirectly influenced by the alumina particles, due to their role in enhancing the *in-situ* dislocation density of the matrix.

V. CONCLUSIONS

DSC-AI samples containing relatively large volume fractions (34 and 37 vol pct) of submicron alumina particles were tested in compression between 25 °C and 600 °C at relatively high strain rates (10^{-3} – 1 s^{-1}) typical of forming operations. These composites exhibit an enhanced flow stress

when compared to pure aluminum under similar testing conditions, but a similar temperature and strain-rate sensitivity. The enhanced flow stress of the composites can be attributed to direct strengthening due to load sharing between the particles and the matrix. However, the *in-situ* matrix flow stress (calculated from the CSC model) is still significantly higher than for annealed and cold-worked aluminum; this is explained by considering indirect strengthening resulting from a particle-induced increase in the density of thermal and plastic mismatch dislocations. Analysis of the data indicates that the micromechanisms leading to the temperature and strain-rate dependence of flow in these DSC-AI materials are the same as in pure aluminum, *i.e.*, forest dislocation interactions. Thus, under the present testing conditions, the mechanical behavior of these DSC-AI materials is more similar to that of metal-matrix composites than to that of dispersion-strengthened aluminum. The high strength of DSC-AI is a combination of load sharing and forest hardening, with the latter mechanisms masking the effects of direct dispersion strengthening operative at lower deformation rates typical of creep deformation.

ACKNOWLEDGMENTS

This study was conducted with the support of the United States Department of Energy through an SBIR subcontract from Chesapeake Composites Corp. (Grant No. DE-FG02-99ER82763).

REFERENCES

1. E. Arzt: *Acta Mater.*, 1998, vol. 46, pp. 5611-26.
2. R.B. Calhoun and D.C. Dunand: in *Comprehensive Composite Materials*, A. Kelly and C. Zweben, eds., Elsevier Science, New York, NY, 2000, vol. 3, pp. 27-59.
3. A.M. Brown and E.M. Klier: U.S. Patent No. 5,511,603, 1996.
4. A.M. Redsten, E.M. Klier, A.M. Brown, and D.C. Dunand: *Mater. Sci. Eng.*, 1995, vol. A201, pp. 88-102.
5. A.M. Jansen and D.C. Dunand: *Acta Mater.*, 1997, vol. 45, pp. 4583-92.
6. D.C. Dunand and A.M. Jansen: *Acta Mater.*, 1997, vol. 45, pp. 4569-81.
7. T.W. Clyne and P.J. Withers: *An Introduction to Metal Matrix Composites*, Cambridge University Press, Cambridge, United Kingdom, 1993, pp. 117-58.
8. B.Q. Han and T.G. Langdon: *Mater. Sci. Eng.*, 2002, vol. A322, pp. 73-78.
9. S. Spigarelli, M. Cabibbo, E. Evangelista, and T.G. Langdon: *Mater. Sci. Eng.*, 2002, vol. A328, pp. 39-47.
10. M. Kouzeli and D.C. Dunand: *Acta Mater.*, in press.
11. S.L. Semiatin and J.J. Jonas: *Formability and Workability of Metals. Plastic Instability and Flow Localisation*, ASM, Metals Park, OH, 1984.
12. C.H. Karnes and E.A. Ripperger: *J. Mech. Phys. Solids*, 1966, vol. 14, pp. 75-88.
13. U.F. Kocks, A.S. Argon, and M.F. Ashby: in *Thermodynamics and Kinetics of Slip*, B. Chalmers, J.W. Christian, and T.B. Massalski, eds., Pergamon Press, Oxford, United Kingdom, 1975.
14. H.J. Frost and M.F. Ashby: *Deformation-Mechanism Maps. The Plasticity and Creep of Metals and Ceramics*, Pergamon Press, Oxford, United Kingdom, 1982.
15. U.F. Kocks: *Mater. Sci. Eng.*, 2001, vol. A317, pp. 181-87.
16. L.F. Mondolfo: *Aluminum Alloys: Structure and Properties*, Butterworth & Co., London, 1976.
17. U.F. Kocks: *J. Eng. Mater. Technol.*, 1976, vol. 98, pp. 76-85.
18. S. Yoshida and N. Nagata: *Trans. Nat. Res. Inst. Met.*, 1967, vol. 9, pp. 20-29.
19. M.F. Ashby: in *Strengthening Methods in Crystals*, A. Kelly and R.B. Nicholson, eds., Elsevier, Amsterdam, 1971, pp. 137-92.
20. M. Kouzeli and A. Mortensen: *Acta Mater.*, 2002, vol. 50, pp. 39-51.